POLITECNICO DI TORINO
Repository ISTITUZIONALE

Toward brain-heart computer interfaces: A study on the classification of upper limb movements using multisystem directional estimates

(Article begins on next page)

12 June 2023

Toward Brain–Heart Computer Interfaces: a Study on the Classification of Upper Limb Movements using Multisystem Directional Estimates

Vincenzo Catrambone[*]**, Giuseppe Averta, Matteo Bianchi, & Gaetano Valenza**

Department of Information Engineering & Bioengineering and Robotics Research Center E. Piaggio, School of Engineering, University of Pisa, Pisa, Italy

E-mail: `vincenzo.catrambone@ing.unipi.it`

1 February 2021

Abstract.   *Objective:* Brain–computer interfaces (BCI) exploit computational features from brain signals to perform a given task. Despite recent neurophysiology and clinical findings indicating the crucial role of functional interplay between brain and cardiovascular dynamics in locomotion, heartbeat information remains to be included in common BCI systems. In this study, we exploit the multidimensional features of directional and functional interplay between electroencephalographic and heartbeat spectra to classify upper limb movements into three classes.
Approach: We gathered data from 26 healthy volunteers that performed 90 movements; the data were processed using a recently proposed framework for brain–heart interplay (BHI) assessment based on synthetic physiological data generation. Extracted BHI features were employed to classify, through sequential forward selection scheme and k-nearest neighbors algorithm, among resting state and three classes of movements according to the kind of interaction with objects.
Main results: The results demonstrated that the proposed brain–heart computer interface (BHCI) system could distinguish between rest and movement classes automatically with an average 90% of accuracy.
Significance: Further, this study provides neurophysiology insights indicating the crucial role of functional interplay originating at the cortical level onto the heart in the upper limb neural control. The inclusion of functional BHI insights might substantially improve the neuroscientific knowledge about motor control, and this may lead to advanced BHCI systems performances.

1. Introduction

1.1. Somatomotor and Central Autonomic Network dynamics

Physical exercises and locomotion provoke complex reactions at the autonomous nervous system (ANS) level [1], and movement-related changes in ANS dynamics include respiration, heartbeat, and blood pressure [2]. Indeed, emotionally-driven behaviors, aggressive/defensive responses, and human physical performances are characterized by a contextual activation of both a somatomotor and autonomic neuronal pathways, which indicate the continuous brain–heart coupling underlying physiological conditions [2]. Further, there are evidences provided by medicine studies of an autonomic-cognitive association involving patients with cognitive disorders. Interestingly, in [3] authors found that the cognitive process of "expectancy," which accompanies motor inhibition, leads to an autonomic reaction that is vagally driven; similar behaviors have been observed in "attention" tasks. In [4], authors studied this vagal response and asked if the detected decrease in the heart rate was caused by a cognitive "expectancy" process, or as a result of the motor inhibition and muscle "quiescence" [5].

From anatomical and functional perspectives, such interactions have been hypothesized as being caused by the superimposition of two systems with some common neural circuits at the central nervous system (CNS); however, a considerable amount of details remain unknown and largely unexplored. In the past, it was believed that the coupling between the somatomotor and autonomic neural pathways was achieved by integrating some node that processes information from the two systems that were considered to be independent. Later, multiple studies discussed the existence of an integrated network projecting on both autonomic (viscera) and somatomotor (muscle–skeleton) efferents. Experiments conducted on humans and animals proved the existence of such a network, which at anatomical level involves the periaqueductal gray matter, nuclei from medulla, hypothalamus, and amygdala, all of which have direct neuronal projections on both the somatomotor and autonomic systems [2]. This circuitry may have different internal nodes specific to certain activities and behaviors, and it is similar to the networks involved in other physiological reflexes. All these regions are part of the so-called central autonomic network (CAN) [6–10] that is defined as the anatomical set of brain areas involved in interactions between the CNS and the ANS; such a functional interaction is commonly defined as the brain–heart interplay (BHI). Indeed, regions such as the ventral medial prefrontal, insular, and parietal cortices with limbic structures including the cingulate cortex, the medial temporal lobe, the amygdala, and the hippocampus are associated with autonomic responses and motor control [1, 11, 12]. A specific oscillation at $0.1 Hz$ originating in the midcingulum, a region involved in motor control functions, has been found to modulate heart rate [13].

It is also worth mentioning that evidences from pathological conditions have indicated the importance of some specific cortical regions. Specifically, [14] reviews the role of ANS in Tourette's syndrome, pointing out that the manifestation of the tic is often bounded to a sympathetic overactivity and a lack of inhibition within a cortico-striato-thalamo-cortical circuit. This is the same region that is critical for coordination and control of fine motor

actions [14]. Further, it has been proved that the autonomic system is activated at an early stage for energy and oxygen recruitment, and for muscle preparation [1]. The autonomic activation occurs independently either in the presence of an actual movement performance or only in a motor imagery case [15]. All these evidences point to the intense functional interplay between ANS and somatomotor cortex.

1.2. Functional Brain–Heart Interplay estimation

The functional interaction between CNS and ANS has been investigated from a methodological viewpoint by employing a variety of signal processing tools to find a quantitative valuation of how the brain and heart interact dynamically. Proposed methods range from measurements adapted to BHI estimation, such as quantification of information transfer from one signal to another [16]; nonlinear convergent cross mapping [17]; estimation of linear and nonlinear cross-system relationship through maximal information coefficient [18, 19]; joint symbolic analysis [20]; or inferring causality exploiting Granger causality index [21]. Moreover, we recently proposed an ad-hoc computational model of the joint activity of the brain and the heart, represented by EEG and HRV series, which gave us the opportunity to quantify their mutual interaction disentangling the components from two opposite directions (i.e., from-brain-to-heart and from-heart-to-brain) in several frequency domains [22]. These exemplary studies investigated neuro-cardiovascular physiology under different physiological and pathological conditions.

1.3. Neuroscience of upper limb movements

Neuroimaging [23] and electrophysiology tools [24–26] have been used in the decades to study the neurophysiology of motor execution and control. In particular, the upper limb movement has been characterized from a kinematics and dynamics viewpoint [27–31], and from a neurological and cognitive one [32, 33]. The analysis has been conducted via experimental paradigms involving four different categories of motor elicitation: execution, planning, observation, and imagery [34, 35], with differences provided by the time length of the stimulation and the artefact-related issues [36].

In the EEG framework, time-frequency analyses are effective for identifying parts of motor control neurophysiology, characterizing scalp regions such as parietal, premotor, prefrontal, and central neural cortices as the most involved in upper limb movements tasks [24, 37–39], and in particular, in determining the α, β, and γ frequency bands [40–44].

Object interaction-based description of upper limb movements is due to neuroscientific studies results. Neuro-psychological and behavioral criteria have been established to classify movements involving the upper limb, and in particular, the hand [32,45,46], into three classes: movements that do not involve the use of any object (intransitives); movements in which the action is directed towards the use of a single object (transitives); and finally, movements in which the interaction with the final object is mediated using another intermediate object (tool-mediated) [30]. This classification has been already employed to successfully disentangle the

topographical organization of brain dynamics in functional studies [47], or to unveil some mechanisms underpinning upper limb biomechanics [30].

Heartbeat dynamics have also been investigated in motor control tasks. Changes in heart rate variability (HRV) were identified during physical activity, particularly an abrupt decrease in the high frequency (HF) power, whereas no significant changes were found in the ration between low frequency and HF powers, LF/HF) [48]. These finding were corroborated by analyses performed by [49], where the authors also discussed on the LF stability during physical activity which was observed to be absent when exercises were performed in a sitting or supine positions [49]. The HRV spectral estimations maintain their reliability when low-intensity physical exercises are performed, and they lose information, particularly in the LF band at higher intensities [49, 50]. As a matter of fact, the ANS being triggered by motor imagery in healthy subjects has been known for many years [51, 52], and beside what associated with energy recruitment, the involvement of ANS in motor control has been argued being related to the emotional and cognitive significance of the movement itself, and to a generalized common activation of CNS and ANS during motor observation and motor imagery [12].

1.4. Hybrid Brain–Computer Interfaces

We recently proposed an approach using high-density EEG system to perform a classification task that disentangles three classes of motor imagery movements divided with respect to their interaction with objects. We employed a subset of electrodes located bilaterally in the parietal, central, and prefrontal lobes, and focused on only the α, β, and γ bands [36]. We proved that this information subset was sufficient to perform classification with recognition accuracy comparable to those achieved using an entire EEG recording [36] with a value as high as 78%.

Such approach is the typical one employed in so-called brain-computer interfaces (BCI), neural interfaces not relying on normal physiological brain pathways to communicate to peripheral nerves and systems [53]. Although several BCI systems have been developed and are daily used by patients worldwide, issues were raised about BCI versatility [54]. The main two issues are the "BCI illiteracy", according to which approximately 20% of people is not able to reach acceptable performances with BCI systems based on motor imagery [54], and the inter subject non-stationarity: BCI systems are not able to appropriately perform due to inter-subject differences in terms of brain patterns [53, 54]. For these reasons, novel BCI approaches have been proposed by combining classical brain signals (e.g., EEG), with other series, particularly, but not limited to, the physiological ones. Such systems have been defined as "hybrid-BCI" [55], theorizing the feasibility of an artificial system considering heart dynamics as an added feature in BCI scenario [53, 55].

1.5. Objective of the Study

As motor control involves coupled functional activity in the brain and cardiovascular dynamics, it is reasonable to hypothesize that a functional BHI estimation might be crucial for enhancing current BCI systems. Indeed, to the best of our knowledge, the functional
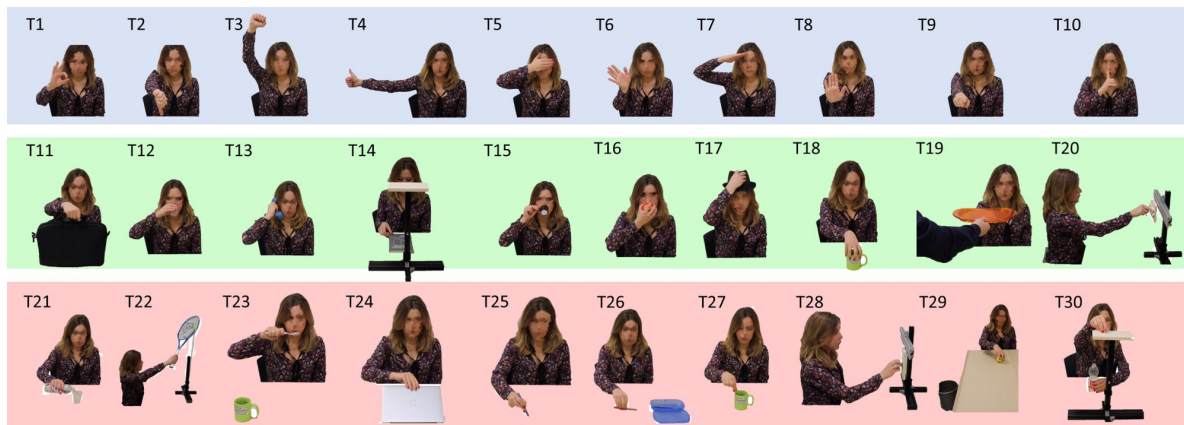
Figure 1. Graphical representation of the 30 movements included in the experimental protocol. The first 10 actions (blue background) belong to the *intransitive* class, movements from the 11th to the 20th constitute the *transitive* class (green background), and the last 10 images represent the tasks belonging to the *tool mediated* class (red background).

interplay between the brain and the heart in motor imagery and, more in general, in motor control tasks has not been investigated yet. To overcome this limitation, we aim to investigate the directional functional BHI in healthy subjects performing upper limb motor imagery and move towards Brain-Heart Computer Interface (BHCI) systems. We show how BHI information can be exploited to automatically recognize the subject's interaction with objects while providing neurophysiological insights. We built on our previous findings using EEG information exclusively [22] and extend the framework at a brain–heart level, demonstrating that the proposed BHCI algorithm achieves a recognition accuracy as high as 95%.

2. Materials and Methods

2.1. Experimental dataset

A total of 26 healthy subjects (all right-handed; 16 females and 10 males; average age: 26.6 years) provided informed consent and volunteered to participate in the study. Experiments were conducted in the laboratories of the University of Pisa. After an initial 5-minutes resting state, in which subjects were comfortably sit on chair with eyes open and in a steady position, participants were asked to perform 30 different right upper limb movements, each repeated three times, resulting in a grand total of 90 different executions per subject. The 30 different tasks considered in this study were suitably selected to cover the three main classes discussed in the Introduction: 10 *intransitive* tasks, e.g., point at something straight ahead with an outstretched arm with the right index finger; 10 *transitive* actions, e.g., reach and grasp an apple, mimic biting and place it back in the initial position; and finally, 10 *tool-mediated* movements, e.g., reach and gasp a bottle, mimic pouring water into a real glass, and place the bottle back in the initial position. The performance of different movements belonging to each class, instead of more classical protocol with several repetitions of the same task, was made necessary since our aim was to focus on the physiological correlates of the classes, avoiding

Figure 2. Exemplary experimental setup. High-resolution EEG sensors and active optical markers are mounted on the subject for motion tracking.

movement-specific confounding factors. A graphical representation of the performed actions is shown in Figure 1.

All movements were carefully explained and mimed to the participants by an operator at the beginning of the experiment. A quick reminder on the specific task to be performed was also provided before each single movement execution. The experimental procedure comprised the repetition of a three blocks scheme for each of the 90 movements (see Figure 3); in particular, participants fulfilled a 3 seconds motor planning state, while maintaining a predefined steady position, and then, they performed the actual planned movement, concluding it in the initial steady position, which they held for additional 3 seconds, before moving on to the next task.

The actual motion execution did not have a predefined time length, and therefore, volunteers were free to perform the tasks at their own pace (time range for all movements and subjects was $[9 - 20]$ seconds). To discriminate the three classes of movements from the resting state, in which subject were not moving neither planning a movement, we divided the 5-minute resting state in 30 non-overlapping segments. This allowed us to have 30 different repetitions of resting state to be included in the classification process (see Figure 3).

The experimental protocol was approved by the Area Nord–Ovest Toscana ethical committee.

Electrophysiological signal were gathered continuously at a sampling frequency of 500 Hz using a EGI Polygraph Input Box (Electrical Geodesics Inc., Eugene, OR, USA) that comprises a high-density EEG system equipped with 128-channels, two-leads ECG, and a single-lead EMG placed on the neck bases, to acquire movements artefacts. Concurrently, we employed a 3D motion tracking system with an active marker (Phase Space, PhaseSpace Inc., San Leandro, CA, USA) to record kinematic data, exploited in other studies [30]. Exemplary experimental setup is shown in Figure 2.

The analysis pipeline was applied to the initial 3-s motor planning phase preceding each movement realization, and thus, it is movement-related artifact free, and most importantly, it focuses on a motor planning cognitive condition.
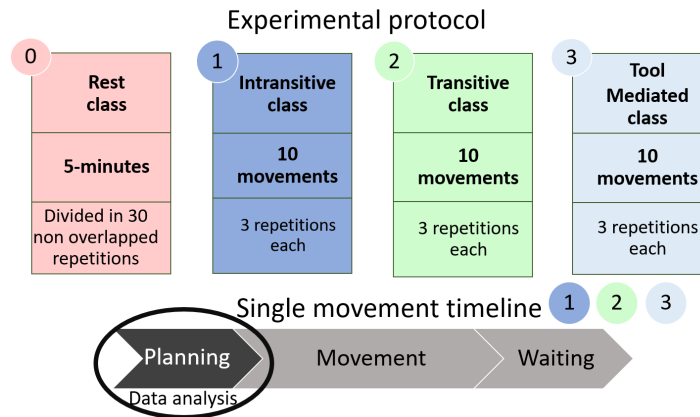
Figure 3. Logic scheme of the experimental protocol timeline comprising three repetitions of 30 different tasks, equally divided in transitive, intransitive, and tool-mediated movements. Each task included a first motor planning phase, an actual movement recording, and a final steady state in which subject were waiting for the next movement. The highlighted window is the one used in the analysis.

2.2. Signal preprocessing

The EEG series were preprocessed by applying the HAPPE pipeline, which is thoroughly described in [56]. In brief, a normalized joint probability of the average log–power from 1–70 Hz is calculated, and channels exceeding the external tails of 1% of the distribution are marked as bad channels and rejected for the following analysis.

A spherical interpolation algorithm that exploits neighbor EEG data was implemented to recover the rejected channels. The EEG oscillations below 1 Hz, and electrical noise at a network frequency of 50 Hz and its harmonic at 100 Hz were filtered out by employing multitaper regression [56]. The EEG artefacts rejection was performed using a wavelet-enhanced ICA–based algorithm that can detect and reject muscular and ocular activities and discontinuities. Further, this approach includes the use of a machine learning algorithm applied to ICA derived components [56]. Eventually, the EEG series were re-referenced to the time varying average from all channels (i.e., average referencing).

From the ECG series, the R-peaks were detected through the well-known Pan-Tompkins algorithm [57]. An online error detection and correction analysis pipeline performing point-process statistics including log-likelihood prediction was implemented on the RR-series, which helped avoid possible physiological (e.g., ectopic beats) or algorithmic (e.g., peak mis-detection) artefacts [58]. Finally, the processed segments were visually inspected before enrolment for further analyses.

Spectral Analysis: The power spectral density (PSD) of each EEG series was estimated by applying the Welch method. We employed a Hamming window of 500 samples ($1sec$) with a 75% overlap. We extracted the PSD exploiting the classical EEG frequency ranges splitting the $\delta \in [1-4Hz)$, $\theta \in [4-8Hz)$, $\alpha \in [8-12Hz)$, $\beta \in [12-30Hz)$, and $\gamma > \in [30-70Hz]$ frequency bands.

For PSD extraction from HRV series, we employed a smoothed pseudo-Wigner–Ville

distribution method (SPWVD) [59], which estimates PSD with a relatively low variance, and it has independent control of the filtering in the time and frequency domains [60]. In brief, WV can be defined as the Fourier transform of the continuous autocorrelation function, which is also referred to as the central covariance function [59].

For each motor task, we estimated the PSD in $3sec$ while anticipating the actual movement performance; thus, we focused our analysis on the cognitive motor planning phase.

2.3. Estimation of Functional Brain–Heart Interplay

We quantify the functional BHI using the synthetic data generation model, proposed in [22]. Formally, the model represents the EEG series according to the oscillators devised in [61]:

$$EEG(t_n) = \sum_{j=1}^{K} a_j(t_n) sin(\omega_j t_n + \phi_j) \tag{1}$$

where $K = 5$, $j \in \{\delta, \theta, \alpha, \beta, \gamma\}$, ω_j is the main oscillation associated with each EEG frequency band, and the amplitudes $a_j(t_n)$ are modeled through a first-order autoregressive (AR) model with an exogenous input:

$$a_j(t_n) \quad = \quad \eta_j a_j(t_{n-1}) \quad + \quad \xi_j(t_{n-1}) \quad + \quad \Psi_j\big(t_{n-1}|P_{B_C}(t_{n-1}), C_{B_C \to j}(t_{n-1})\big) \tag{2}$$

where $B_C \in \big\{LF = [0.04, 0.15]Hz, HF = [0.15, 0.4]Hz\big\}$, η_j is a constant for the AR process, $\xi_j(t_{n-1})$ is a Gaussian white noise term, $P_{B_C}(t_{n-1})$ is the PSD calculated in the B_C band from the HRV series at time t_{n-1}, and $C_{B_C \to j} \equiv C_{Heart \to Brain}$ is the actual coupling strength in the direction from-heart-to-brain, specifically at the B_C frequency band for HRV series and at the j band for the EEG series. It is then possible to define the heart-to-brain coupling function as follows:

$$\Psi_j(t_{n-1}) = C_{B_C \to j}(t_{n-1}) \times P_{B_C}(t_{n-1}|\mathcal{H}_{t'}^C) \tag{3}$$

with heartbeat history $\mathcal{H}_{t'}^C$.

The RR series are modeled by using the integrate and pulse frequency modulation model proposed in [62]:

$$RR(t) = \sum_{k=1}^{N} \delta'(t - t_k) \tag{4}$$

where δ' indicates a Dirac delta function, t is the continuous time, and t_k is the time of the k-th heartbeat occurrence identified as follows:

$$1 = \int_{t_k}^{t_{k+1}} [HR + m(t)] dt \tag{5}$$

where HR is the mean heart rate expressed in Hz. The $m(t)$ function represents an autonomic activity function, which is defined as

$$m(t_n) = C_{LF}(t_n) \sin(\omega_{LF} t_n) + C_{HF}(t_n) \sin(\omega_{HF} t_n) \tag{6}$$

$$C_{LF}(t_n) = C_{LF_0} + \Psi_{LF}\big(t_{n-1}|P_j(t_{n-1}), C_{j\to LF}(t_{n-1})\big) \tag{7}$$

$$C_{HF}(t_n) = C_{HF_0} + \Psi_{HF}\big(t_{n-1}|P_j(t_{n-1}), C_{j\to HF}(t_{n-1})\big) \tag{8}$$

where ω_{LF} and ω_{HF} are the main oscillations associated with each HRV frequency band, $P_j(t_{n-1})$ represents the PSD in the j band from the EEG series at time t_{n-1}, C_{LF_0}, and C_{HF_0} are constant terms associated with the LF and HF bands, and $C_{j\to B_C} \equiv C_{Brain\to Heart}$.

The brain-to-heart coupling function $\Psi_{B_C}(t_{n-1})$ is defined as follows:

$$\Psi_{B_C}(t_{n-1}) = C_{j\to B_C}(t_{n-1}) \times P_j(t_{n-1}|\mathcal{H}_{t''}^B) \tag{9}$$

where B_C and j as in 2; $\mathcal{H}_{t''}^B$ is the brain activity history. Thus, $C_{B_C\to j}$ represents the actual coupling index in the direction from-brain-to-heart, specifically from the B_C frequency band of HRV series, to the j band of the EEG.

To summarize, the time-varying directional BHI biomarkers are $C_{B_C\to j}(t_n)$ and $C_{j\to B_C}(t_n)$, which represent the instantaneous estimation of the heart-to-brain and the brain-to-heart interactions, respectively. The key idea behind this model design is that the electrophysiological activities of the two systems are not independent one from the other, and the introduced coupling terms mediate such interactions. For example, a positive value of the $C_{\delta\to LF}(t_n)$ would indicate that the δ band of the EEG at time t_n is exerting a positive influence (i.e., leading to a linearly proportional increase) in the PSD of the HRV series in the LF-band.

The derivation of the entire family of BHI biomarkers through inverse model formulation has been described in [22], and a easy-to-use MATLAB implementation is freely available at [63]. Through this framework, we derived directional BHI indices listed in Table 1.

2.4. Statistical analysis

We investigated significant group-wise changes between the four experimental cases, i.e., resting state, and intransitive, intransitives, and tool mediated actions. To this end, a between-session statistical comparison was performed for each BHI index, namely LF→brain, HF→brain, brain→LF, and brain→HF, through a Friedman non-parametric test for paired samples. Experimental tasks belonging to the same class were grouped and a median value was extracted for each subject. Thus, a single median for each subject was calculated across the 30 instances of actions belonging to each class (i.e., 10 movements $\times 3$ repetition). Significance was chosen at 5%, and p-value correction for multiple comparison was performed through a permutation test with 1000 permutations. A cluster-mass permutation correction

Table 1. BHI indices extracted through the model.

Index	From	Band	To	Band
$C_{Brain_j\to Heart_{B_C}}$	Brain	$\delta, \theta, \alpha, \beta, \gamma$	Heart	LF, HF
$C_{Heart_{B_C}\to Brain_j}$	Heart	LF, HF	Brain	$\delta, \theta, \alpha, \beta, \gamma$

was applied to assess the physiological plausibility of the results [64]. All the results are plotted as topographic distributions of significant p-values from the associated tests. The subject-wise median values for all experimental phases, on which the statistical tests have been performed, have been represented as well.

2.5. Classification algorithm

We implemented a four-class K-nearest neighbor (K-NN) classifier that has been largely employed in previous studies [65, 66]. K-NN is a supervised non parametric algorithm that from a series of labeled training samples finds K points $x(r), r = 1, ..., k$ that have the lowest distance (in the simplest case Euclidean; however, it can use other distance definitions) to any specific query observation x_0. The classification of the query observation x_0 is then provided by the most frequent class among the K-neighbors.

In classification tasks, overfitting problems are always a risk that needs to be avoided; this risk is even higher when a high number of features is used to train a relatively limited number of observations. In this study, we choose to overcome this issue by performing a dimensionality reduction through principal component (PC) analysis, and by running a classification algorithm with an increasing number of PCs (set according to the increasing variance ratio) according to a classical *sequential forward selection* (SFS) scheme [67]. We did not use the validation set to perform PCA; it was implemented only on the training set, and thus, it follows that the validation set was transformed into PCs using weights calculated only from the same training set used by the classifier.

We employed a specific cross-validation (CV) scheme to assure the out-of-sample prediction accuracy of the system and avoid potential bias. Since the resting class does not have different movements, but only 30 repetition of the same resting condition, those 30 segments were divided in 10 folds of 3 repetitions each, thus allowing the algorithm to have 4 classes completely balanced in each fold. The CV pipeline was iteratively repeated 10 times, each made of a dataset division in the testing set, which comprised all repetitions for all subjects of one action for each class (i.e., a total of 26 subjects × 3 repetitions × 4 classes ≃ 312 points), whereas the training set included the remaining data (i.e., a total of 9 folds × 26 subjects × 3 repetitions × 4 classes ≃ 2808 points). The input feature set was split iteratively into a validation set and a training set (see Figure 4). In particular, we repeated classification trials with a different features set, provided by the increasing number of PCs enrolled at each iteration; further, at each iteration, we derived the final accuracy using the CV procedure and averaging across the 10 repetitions. The employed CV procedure takes inspiration from both the K-fold [68] and leave-one-out (LOO) [69] algorithms. Analogously to K-fold, our CV pipeline divides the dataset into 10 folds, leaving one out for validation set and exploiting the rest as training set, but the folds are divided in order to assure that three repetitions of an action for each class are contained in each fold, in each CV repetition one action of each class is left out (in analogy with LOO). This procedure allows for the out-of-sample prediction accuracy of the system and avoid potential bias, maintaining the balance among classes both in the training and testing sets.
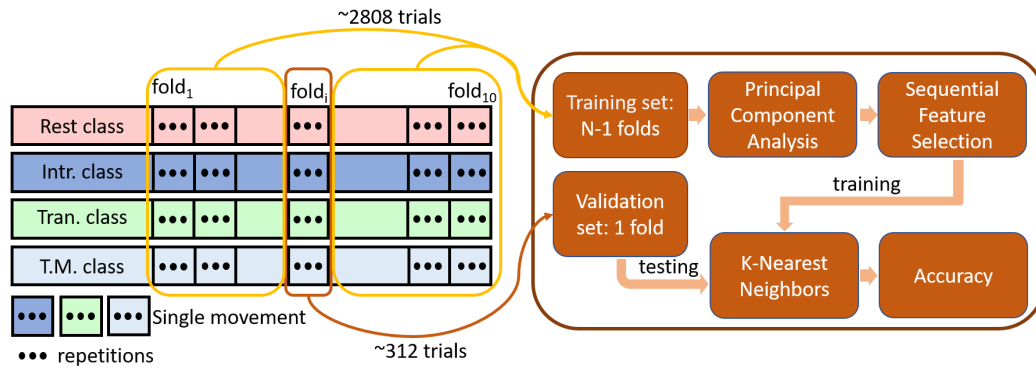
Figure 4. Block scheme of the data analysis and classification pipeline.

As already discussed, this study employs BHI indices to automatically recognize classes belonging to a series of movements that the subjects were going to perform. BHI indices are derived from the time window before actual movement execution wherein participants were supposed to plan the following action. In particular, the changes here are evaluated in terms of classification accuracy with respect to the direction of the BHI, i.e., from-brain-to-heart or vice versa.

We investigated how BHI directionality and HRV frequency band affect motion classification tasks, and considered four different input datasets:

- BHI from HRV-LF band of cardiac activity to brain: LF→brain.
- BHI from HRV-HF band of cardiac activity to brain: HF→brain.
- BHI from brain to HRV-LF band of cardiac activity: brain→LF.
- BHI from brain to HRV-HF band of cardiac activity: brain→HF.

For each of these datasets, a feature vector is created for extracting the median across the time of the BHI estimates for each channel. To reduce the feature space of the machine learning classification task, and thus optimize performances, we selected a subset of EEG bands and electrodes as follows.

In accordance with previous studies [24, 37–39, 70, 71], electrode reduction was performed by selecting only the central, parietal, and prefrontal regions, i.e., a comprehensive amount of 33 electrodes, (Figure 5). For the EEG frequency bands, we limited our analysis to the α, β, and γ ranges, which are commonly considered informative in motor-related tasks [40, 43, 72]. This reduction allowed us to have a total amount of 99 features (33 channels $\times$ 3 frequency bands). Both choices were based on the procedure exploited in our previous study that employs the same dataset with only EEG-derived features [36]. The feature reduction was applied for a future viable implementation, i.e., in a possible BCI scenario where physical and eventually economic constraints pose limits on the number of electrodes used for a wearable implementation.
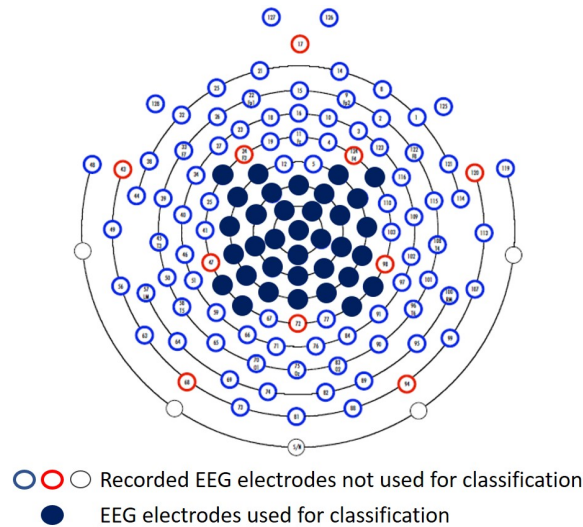
○ ◯ ◯ Recorded EEG electrodes not used for classification
● EEG electrodes used for classification

Figure 5. The 33 electrodes selected as a subset of interest in one of the proposed studies are marked (section 3).

3. Results

3.1. BHI topographic distribution

A topographical representation of extracted BHI indices across the whole scalp (90 EEG electrodes) is presented for each class in figures 9, 6, 7, and 8, respectively. Some remarkable differences seems to be present considering the resting state BHI topographical distribution with respect to the other three classes of actions, all performing motor planning tasks. The figures qualitatively show high similarity among the three classes involving motor planning in the topographic distribution of BHI indices across the scalp for each combination of EEG and HRV frequency ranges and direction considered, even if the tool mediated class have higher BHI values in the direction from-heart-to-brain. The distributions have considerably evident discrepancies in the two opposite directions; particularly in the brain-to-heart indices, which consider the HRV-LF band, and they have always lower values than the other combinations, both in terms of absolute values and signs. The negative sign represents an inverse relationship between the EEG-PSDs and the HRV activity, which implies that an increase in the EEG activity in a given band will entail a decreased power in the HRV-LF band. Conversely, all other BHI indices hold a positive sign, which implies an accordance in the brain and heart behavior.

The heart-to-brain indices depict an overall high similarity between the two considered HRV frequency ranges. In these distributions, an overall ascending radial gradient going from the central brain regions to the most peripheral electrodes in the frontal, occipital, and temporal ones seem to characterize all heart-to-brain BHI indices for all four classes of action represented by the first two rows in figures 9, 6, 7, and 8. In particular, θ EEG band hold the lowest values across the EEG spectrum, while the β band has the highest, and specifically, the bilateral occipital and right frontal areas. The α and γ bands, instead show different behavior
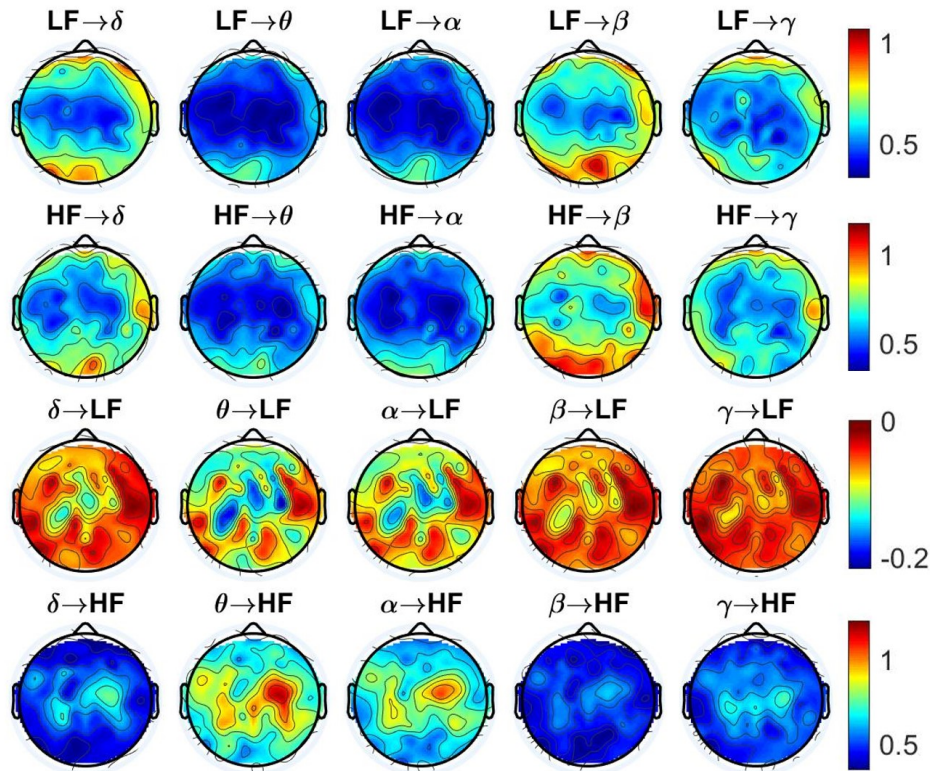
Figure 6. Topographic map of directional BHI indices extracted during motion planning phase of intransitive movements as the median across subjects and actions. Each topoplot represents a specific combination of EEG- and HRV- frequency ranges in one of the directions from-heart-to-brain (first two rows), and from-brain-to-heart (last two rows). Each colorbar refers to the entire row where it is placed.

in the four classes of movements, the former being very low for the three motor planning classes, whereas it seems as high as the β band in the resting trials. The latter behaves in the opposite way, being relatively high in the motor planning phases and remarkably decreasing in the resting phase.

In the opposite direction, i.e., from-brain-to-heart, the two HRV-derived frequency bands show considerably different behavior, both in terms of absolute values of BHI estimation, and in terms of relative topographic distribution. Indeed, the brain-to-HF indices always have considerably higher values with respect to the brain-to-LF indices, as mentioned previously. Moreover, in the brain-to-LF indices, the θ and α EEG bands have the lowest values in their row in figures 6, 7, and 8; whereas this role is for the α and β bands in Figure 9. The color bars of the last row in these figures indicate that the θ and α EEG bands in the brain-to-HF indices highlight the highest BHI estimates, assuming a different range of values in comparison with the other three bands in the motor planning faces (see figures 6, 7, and 8). At a first glance, the two HRV bands seem to show opposite behavior with respect to the five EEG bands in the motor planning phase; however, it must be noticed that in the brain-to-LF combinations, the BHI indices have a negative sign, and thus, it means that in terms of absolute values, the θ and α EEG bands show the strongest BHI estimates again (see figures 6, 7, and 8). In the resting
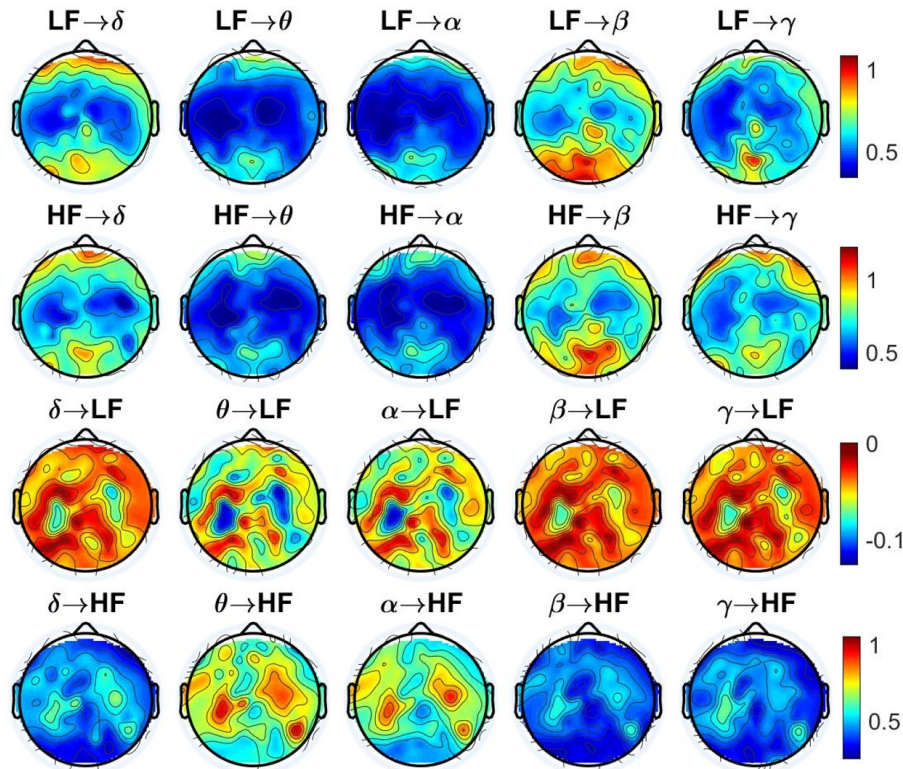
Figure 7. Topographic map of directional BHI indices extracted during the motion planning phase of transitive movements, as the median across subjects and actions. Each topoplot represents a specific combination of EEG- and HRV- frequency ranges in one of the directions from-heart-to-brain (first two rows) and from-brain-to-heart (last two rows). Each colorbar refers to the entire row where it is placed.

state (Fig. 9) a more smooth distribution is depicted, with the highest values among the four classes. In this case the θ and γ bands show the highers values, whereas the α and β bands hold the lowers.

In Figure 10 the results from the group-wise statistical comparison are shown. No difference between the four classes were found in the HF→brain and brain→LF combinations. Considering the LF→brain, many significant regions are depicted in the θ, α and β bands in similar scalp areas. More specifically, these significant clusters are found in the frontal, left (contralateral) prefrontal, central and dorso parietal right (ipsilateral) regions. Regarding the brain→HF combinations, clusters in the dorso-temporal and occipital lobes are found in the δ band, whereas almost the entire scalp is found significant in considering the γ EEG band.
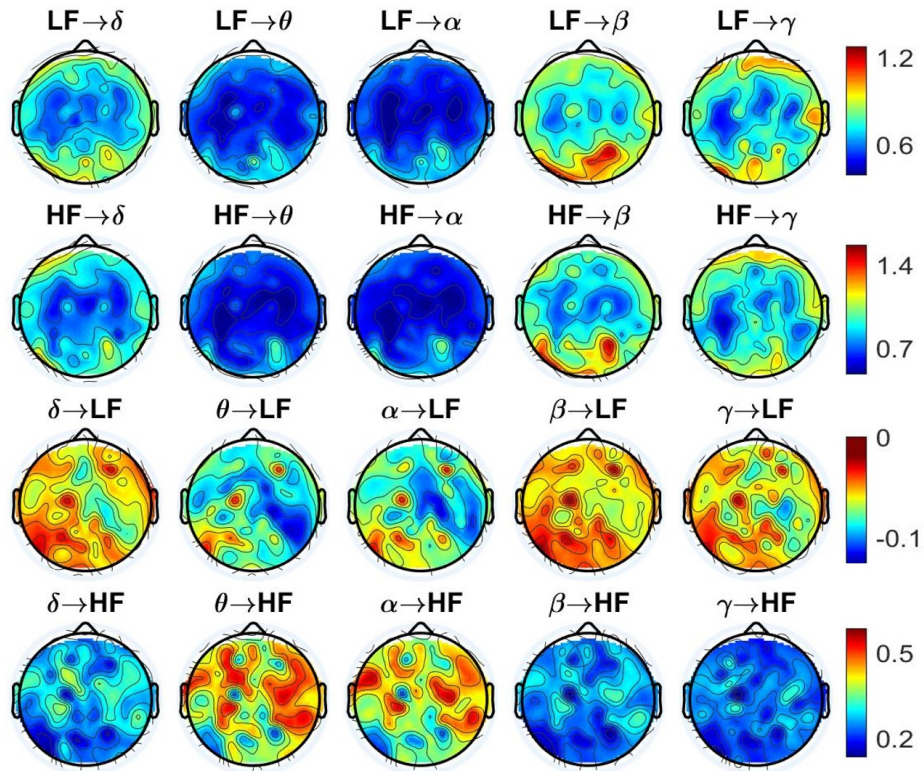
Figure 8. Topographic map of directional BHI indices extracted during motion planning phase of tool mediated movements, as the median across subjects and actions. Each topoplot represents a specific combination of EEG- and HRV- frequency range, in one of the directions from-heart-to-brain (first two rows), and from-brain-to-heart (last two rows). Each colorbar refers to the entire row where it is placed.
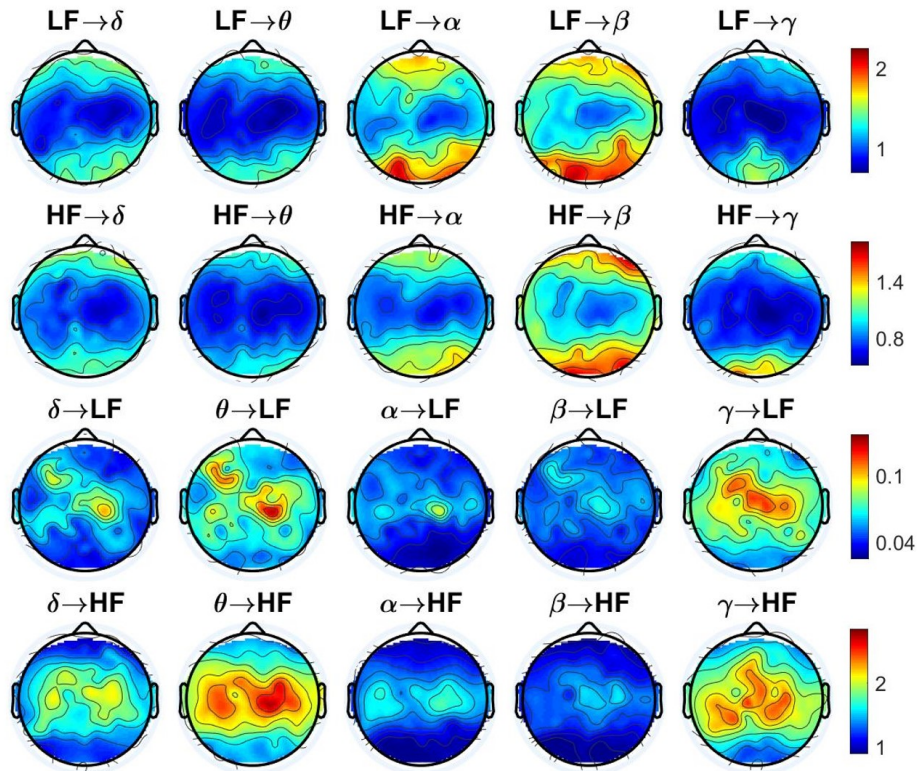
Figure 9. Topographic map of directional BHI indices extracted during resting state, as the median across subjects and actions. Each topoplot represents a specific combination of EEG- and HRV- frequency range, in one of the directions from-heart-to-brain (first two rows), and from-brain-to-heart (last two rows). Each colorbar refers to the entire row where it is placed.
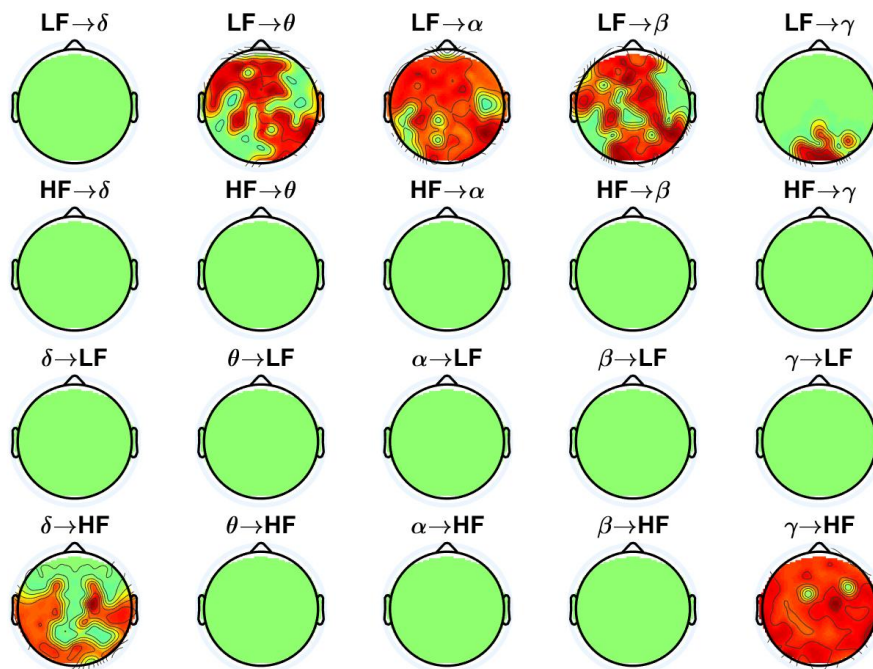
Figure 10. Topographic map of corrected p-values from statistical group-wise Friedman test for paired samples. The test has been applied on the 4 classes of recordings (i.e., intransitives vs transitives vs tool mediated vs rest). Each topoplot represents a specific combination of EEG- and HRV- frequency range, in one of the directions from-heart-to-brain (first two rows), and from-brain-to-heart (last two rows). Green areas represent not significant electrodes, whereas red areas represent corrected p-values statistically significant. Multiple comparison were accounted through permutation tests.

3.2. Classification results

Experimental results are expressed as accuracy trends with respect to the number of selected PCs and are differentiated by movements classes. Figure 11 shows the classification results using LF→brain indices. The pink dashed line represents the true positives rates for resting state segments (rest); blue dashed line refers to the true positives achieved for intransitive movements (intr); green, the percentage of transitive movements that were well-classified (tran); and cyan, the tool-mediated movements correctly classified (t.m.). The balanced accuracy (averaged among positive rates of the four classes) is reported using a continuous red line. The same color code is used in the following representations. The true positive index of the rest class is beyond 80% from 15 principal components (PCs). The other three classes always show an accuracy lower than the first (maximum at $\approx 75\%$). The maximum accuracy achieved considering the average among classes is 76.82%, using 38 PCs out of the initial 99. The classifier needs at least 15 features to achieve an acceptable accuracy beyond 70% on average; further, it is much lower with less PCs, and it decreases when more than 40 features are enrolled. This decreasing trend is attributed to the recognition of the intransitive classes, whereas the rest class shows a plateau that is approximately constant beyond 10 features. This is possibly because of a misclassification between the last two classes (i.e., transitive and tool mediated) that are more similar with respect to the others (both include the use of an object differently from the rest and intransitive, which is an object-free movement). Even if a 76.82% accuracy is not an optimum result in terms of general classification performance of a machine learning application, it is a satisfactory result in the context of BHI-derived analysis and classification, particularly among similar classes.
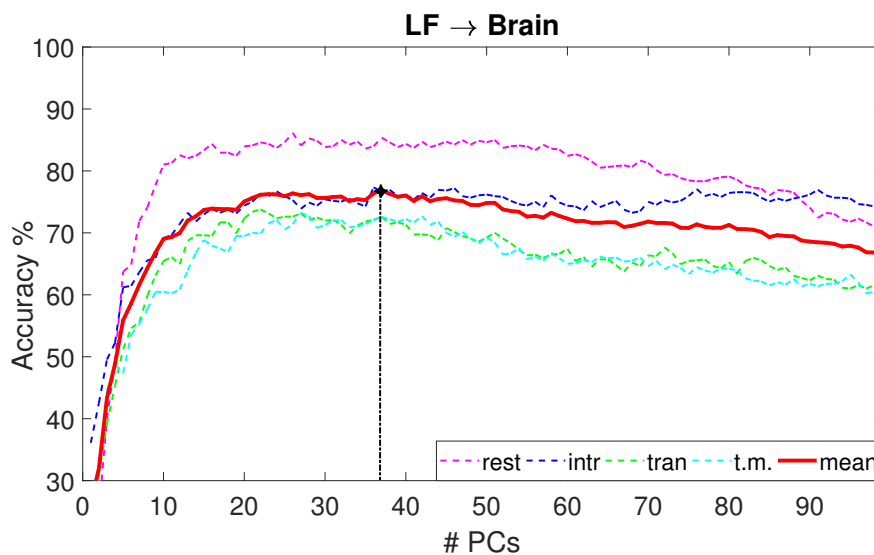

Figure 11. Classification accuracy with respect to the number of principal components (PCs) of the LF→Brain BHI indices considered as input features. The four colored dashed lines denote the single true positives rate for each of the four classes separately, and the continuous red line represents their average accuracy. The black dotted vertical line highlights the point where the maximum average accuracy is achieved.

Figure 12 shows the classification results using HF→brain indices. The figure is considerably similar to the preceding one, in terms of both maximal accuracies and trends with respect to the number of employed PCs. The maximum percentage of corrected classifications is reached for the rest trials (89.841%), whereas the maximum average accuracy achieved is 77.17% with 40 features. Thus, the maximal accuracy is quite higher than the previous classification w.r.t. the rest class; however, it is only slightly higher considering the average. The decreasing course of the true positive rates for the third and fourth class (i.e., transitive and tool mediated) is still present, even if with a lower slope with respect to Figure 11. General classification results obtained with HF→brain BHI indices match the ones obtained by substituting the LF band to the HF band of the HRV.
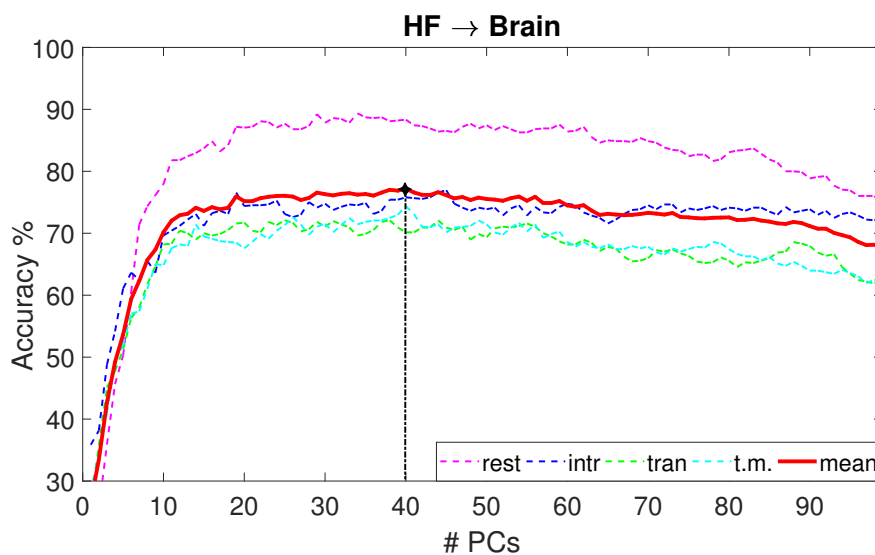

Figure 12. Classification accuracy with respect to the number of PCs of the HF→Brain BHI indices taken as input features. The four colored dashed lines stand for the single true positives rate for each of the four classes separately, the continuous red line represents their average accuracy. The black dotted vertical line highlights the point where the maximum average accuracy is achieved.

Figure 13 shows the classification results employing brain→LF indices. Excellent accuracies are obtained for all four true positives rates, one for each class separately, higher than 85% with more than 17 features. The average rate among them reaches its maximum with 32 PCs and it is equal to 91.27%. The general maximum is achieved in the second class (i.e., intransitives movements), and it is 95.24%. Very high classification results are obtained with 15 features that exceed 80%; with more than 20 PCs, the accuracy seems to remain almost constant. The gap between the true positives rates of the four classes are shorter with respect to the previous two figures (i.e., Fig. 11 and Fig. 12), and they overlap with more than 40 features.

Figure 14 shows the classification results employing brain→HF indices. The figure is considerably similar to the preceding one (Fig. 13), particularly in terms of trends with respect to the number of employed PCs. Indeed, the maximum percentage of corrected classifications
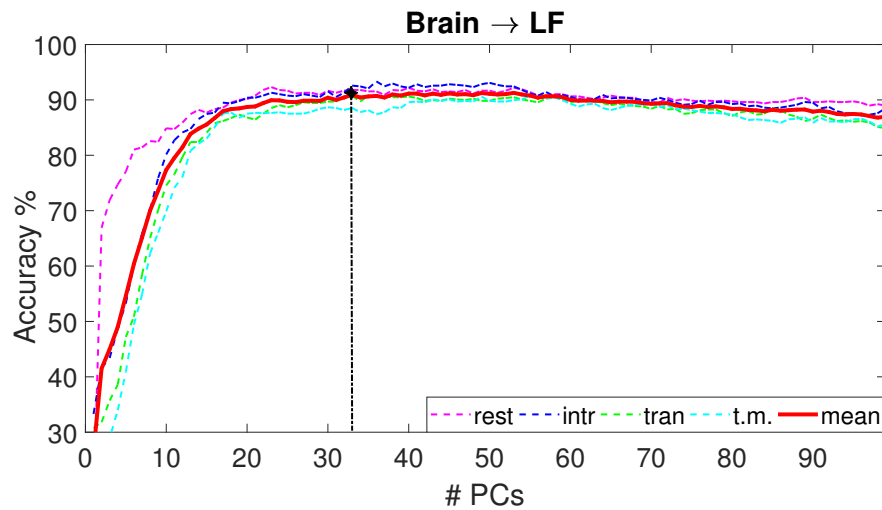
Figure 13. Classification accuracy with respect to the number of PCs of the Brain→LF BHI indices taken as input features. The four colored dashed lines stand for the single true positives rate for each of the four classes separately, the continuous red line represents their average accuracy. The black dotted vertical line highlights the point where the maximum average accuracy is achieved.

is 98.4% for the rest class, whereas the maximum average accuracy is 95.32% with 42 features. Thus, the maximal accuracy is the highest among all classifications, both in terms of average accuracy and maximum values.
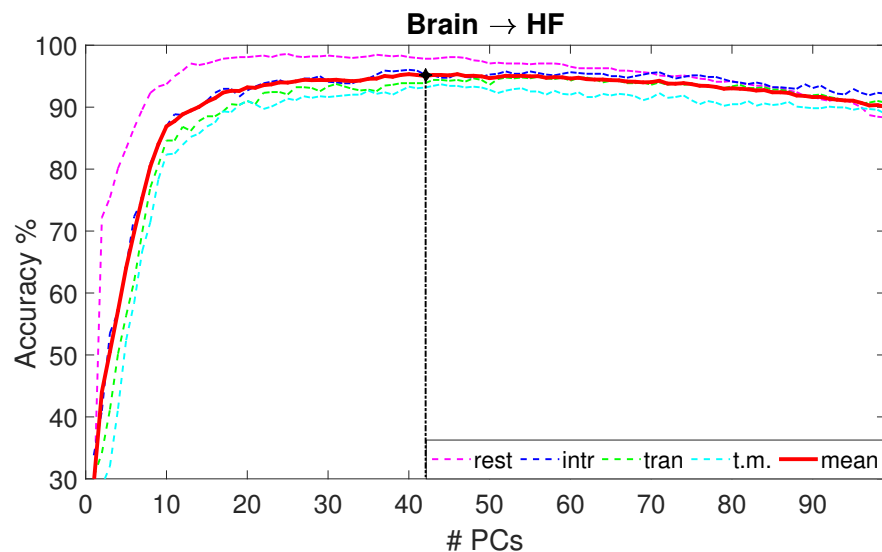

Figure 14. Classification accuracy with respect to the number of PCs of the Brain→HF BHI indices taken as input features. The four colored dashed lines stand for the single true positives rate for each of the four classes separately, the continuous red line represents their average accuracy. The black dotted vertical line highlights the point where the maximum average accuracy is achieved.

Finally, a comparison among the four datasets employed for classification is shown

in Figure 15, where a difference is clearly noticeable. In particular, the brain-to-heart indices lead to a considerably more performing classifier with respect to the opposite BHI direction. The HRV-HF band allows a slightly higher classification accuracy in the brain-to-heart combination, whereas no remarkable differences are highlighted in the opposite case.
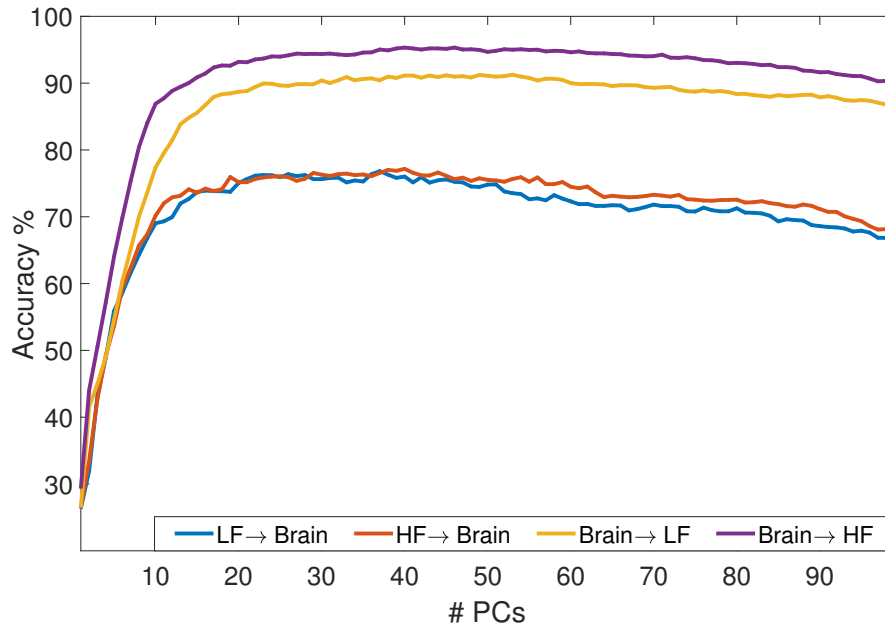

Figure 15. Classification accuracy with respect to the number of PCs considered as input features. The four colored lines indicate the average performance achieved using a different BHI index in the 4-class classification algorithm.

4. Discussion

4.1. BHI estimates as novel BCI features and BHCI systems

To pave the way toward future hybrid BCI applications, theorized by [53, 55], the proposed analysis pipeline employs BHI estimates to classify intransitive, transitive, and tool-mediated movements. The BHI phenomenon is widely known to be involved in the physiologic body processing of emotions [18–21, 73–77], and it has been suggested that the emotional states could affect the BCI performances [78]; furthermore, the development of an emotional-BCI has already been proposed [79]. We prove that it is possible to categorizes upper limb movements, which is a typical BCI application, employing only BHI-derived features; thus, we suggest including BHI quantification in BCI systems.

The proposed study exploited the motor planning phase to anticipate actual motor execution. This approach has been widely used to investigate a crucial cognitive process related to motor control [35, 80, 81], which has a dual advantage of being fundamentally free from motor-related artifacts, and, most importantly in BCI scenarios, it precedes the beginning of the actual motor performance. This allow us to exploit useful information to modulate a motor control strategy.

4.2. BHI directionality

This study provides insights in the directionality of the BHI phenomenon. Results shown in Figure 15 summarize the classifications obtained from the four different combinations of HRV bands and the directionality between the brain and the heart. Further, this figure shows that the from-brain-to-heart direction leads to considerably better results in terms of accuracy, and it exceeds what obtained for the opposite direction by approximately 20%. Moreover, slight differences were reported between the two HRV frequency bands considered in the direction from the brain to the heart, in which the HF band of the HRV leads to better results; whereas no detectable differences were observed in the opposite direction. This result suggests that the way in which the brain processes the interaction with an object strongly affects the communication between the brain and the heart, and, in particular, in the motion planning phase. As a speculation, our results might suggests that the BHI actually change during different kind of motor imagery tasks, and that, in this case, the phenomenon is mainly driven by the CNS. We might conjecture that the importance of the interplay from brain to heart is related to the energy demand or to a finer motor control that is planned.

Furthermore, investigating how to employ the BHI estimates in a BCI application, our results suggest considering the directionality of the BHI and to prefer, in this context, the from-brain-to-heart measurements.

4.3. Classification results

Our classification algorithm scored a maximum accuracy of 95.32% for classifying resting state, intransitive, transitive, and tool mediated movements, which is an outstanding results

using only BHI indices, particularly in the direction from the brain to the vagal HRV frequencies in the HF range. As shown in Figures 11, 12, 13, and 14, resting state is always the most recognized class, whereas movements that do not include the use of an object are always better classified than the other two categories. These results are in agreement with [47] and [36, 82, 83], and they are reasonably linked to the fact that two classes involving object interaction (transitive and tool mediated) are more similar to each other, particularly in terms of neural dynamics underlying the processing. Previous studies using brain dynamics information exclusively showed a classification accuracy of $\sim 80\%$ for a three-class recognition problem including transitive, intransitive, and tool-mediated movements [36, 47]. Such studies highlighted the importance of specific scalp regions and EEG oscillations in specific frequency bands, which constitute the foundations of the feature engineering and selection stage of the proposed BHCI systems.

The significant increase in classification accuracy associated with BHCI with respect to the more standard, EEG-based BCI proposed in [36] may be due to different factors including the exploitation of concurrent EEG and ECG-HRV information, as well as the use of ad-hoc pre-processing and processing procedures needed for the quantification of functional, directional brain-heart interplay. Note also that, differently from [36, 47], this study includes the processing and classification of data gathered in resting state conditions. The feature reduction scheme allows us to obtain the maximum accuracy with almost 40 PCs, even if only 20 PCs were sufficient to obtain 90% of the average accuracy; thus, they sensibly reduce the computational cost of the classification algorithm.

The literature review [24, 37–39, 70, 71] indicates that we need to choose a subset of features a-priori, both in terms of EEG electrodes, selecting those in central, parietal, and prefrontal areas of both hemispheres, and frequency bands, selecting the α, β and γ bands. Furthermore, we implemented a feature selection strategy based on PCA and a SFS scheme. This reductive approach is a key element in real-application systems, where there is a strong quest for wearability and processing acceleration.

5. Conclusion

In this study, we demonstrated that a novel BHI-based classification analysis is effective to automatically recognize different upper limb movements. We recorded EEG and HRV signals during a motor planning paradigm performed by 26 participants. The experimental protocol consisted of resting state along with 30 actions, each repeated three times, with the actions belonging to three motion categories previously described in literature, and classified based on their interaction with the objects, i.e., intransitive, transitive, and tool-mediated. Previous functional neurological studies and motion tracking ones investigated brain activity and motor synergies related to each of these three classes [47]. Moreover, the EEG derived features were already employed in classifying these three categories of movements, highlighting gender related differences [36]. However, to the best of our knowledge, no evidence on BHI data has been provided under this regard, and the classes were not compared to resting state.

Although the functional BHI computation algorithms need to be optimized for a real

BCI scenario, this study represents the first attempt in recognizing movements employing only BHI derived features. Future endeavors will be directed toward the optimization of the algorithmic complexity associated with a BHI estimation from EEG and ECG series, targeting a brain-heart computer interface implementation working online. Moreover, a study on classification interpretability aiming to identify which frequency bands and EEG electrodes are most informative will be pursued as well; this will help devising further feature reduction strategies, as well as providing novel neuroscientific insights on brain- body motor control processes. Further investigations are necessary to characterize BHI physiological and pathological phenomenology in motion-related paradigms, also considering gender differences and other brain dynamics sources.

[1] Collet C and Guillot A 2010 *The neurophysiological foundations of mental and motor imagery* 95–108
[2] Kerman I A 2008 *Experimental brain research* **187** 1–16
[3] Jennings J R *et al.* 1991 *Psychophysiology* **28** 72–85
[4] Jennings J R 1992 *Psychophysiology* **29** 369–383
[5] Hugdahl K 1996 *Current opinion in neurobiology* **6** 252–258
[6] Benarroch E E 1993 The central autonomic network: functional organization, dysfunction, and perspective *Mayo Clinic Proceedings* vol 68(10) (Elsevier) pp 988–1001
[7] Valenza G *et al.* 2019 *Neuroimage* **197** 383–390
[8] Sklerov M *et al.* 2019 *Clinical Autonomic Research* **29** 555–566
[9] Beissner F *et al.* 2013 *Journal of neuroscience* **33** 10503–10511
[10] Valenza G *et al.* 2020 *Journal of the Royal Society Interface* **17** 20190878
[11] Wong S W *et al.* 2007 *Neuroimage* **35** 698–708
[12] Collet C, Di Rienzo F, Hoyek N and Guillot A 2013 *Frontiers in human neuroscience* **7** 415
[13] Pfurtscheller G *et al.* 2017 *Clinical Neurophysiology* **128** 183–193
[14] Hawksley J *et al.* 2015 *Frontiers in neuroscience* **9** 117
[15] Bolliet O *et al.* 2005 *Applied psychophysiology and biofeedback* **30** 11–20
[16] Faes L *et al.* 2015 *Physical Review E* **91** 032904
[17] Schiecke K *et al.* 2019 *Physiological Measurement* **40** 114001
[18] Catrambone V *et al.* 2019 *Entropy* **21** 892
[19] Valenza G *et al.* 2016 *Phil. Trans. R. Soc. A* **374** 20150176
[20] Schulz S *et al.* 2016 *Philosophical Transactions of the Royal Society A: Mathematical, Physical and Engineering Sciences* **374** 20150178
[21] Greco A *et al.* 2019 *American Journal of Physiology-Regulatory, Integrative and Comparative Physiology* **317** R25–R38
[22] Catrambone V *et al.* 2019 *Annals of biomedical engineering* **47** 1479–1489
[23] Lotze M *et al.* 2000 *Neuroimage* **11** 473–481
[24] Avanzini P *et al.* 2012 *PLoS One* **7** e37534
[25] Pfurtscheller G *et al.* 1979 *Clinical Neurophysiology* **46** 138–146
[26] Neuper C *et al.* 2006 *Progress in brain research* **159** 211–222
[27] Lenarcic J *et al.* 1994 *IEEE transactions on systems, man, and cybernetics* **24** 1239–1246
[28] Rau G *et al.* 2000 *Journal of biomechanics* **33** 1207–1216
[29] Lo H S *et al.* 2012 *Medical Engineering and Physics* **34** 261–268
[30] Averta G *et al.* 2017 *Frontiers in Robotics and AI* **4** 37
[31] Averta G *et al.* 2019 *IEEE Transactions on Neural Systems and Rehabilitation Engineering* **27** 1397–1406
[32] Bartolo A *et al.* 2008 *The Clinical Neuropsychologist* **22** 27–45
[33] Buxbaum L J *et al.* 2014 *Brain* **137** 1971–1985
[34] Jeannerod M 1994 *Behavioral and Brain sciences* **17** 187–202
[35] Hanakawa T *et al.* 2008 *Cerebral cortex* **18** 2775–2788

[36] Catrambone V *et al.* 2019 *IEEE Transactions on Neural Systems and Rehabilitation Engineering* **27** 411–418

[37] Caspers S *et al.* 2010 *Neuroimage* **50** 1148–1167

[38] Arnstein D *et al.* 2011 *Journal of Neuroscience* **31** 14243–14249

[39] Molenberghs P *et al.* 2012 *Neuroscience & Biobehavioral Reviews* **36** 341–349

[40] McFarland D J *et al.* 2000 *Brain topography* **12** 177–186

[41] Pfurtscheller G *et al.* 1999 *Clinical neurophysiology* **110** 1842–1857

[42] Ritter P *et al.* 2009 *Human brain mapping* **30** 1168–1187

[43] De Lange F P *et al.* 2008 *Frontiers in human neuroscience* **2** 7

[44] Yuan H *et al.* 2010 *Neuroimage* **49** 2596–2606

[45] Petreska B *et al.* 2007 *Progress in brain research* **164** 61–83

[46] Canzano L *et al.* 2016 *Frontiers in human neuroscience* **10**

[47] Handjaras G *et al.* 2015 *Human brain mapping* **36** 3832–3844

[48] Yamamoto Y *et al.* 1991 *Journal of applied physiology* **71** 1136–1142

[49] Perini R and Veicsteinas A 2003 *European journal of applied physiology* **90** 317–325

[50] Michael S *et al.* 2017 *Frontiers in physiology* **8** 301

[51] Lang P J 1979 *Psychophysiology* **16** 495–512

[52] Jones G E and Johnson H J 1980 *Psychophysiology* **17** 339–347

[53] Choi I *et al.* 2017 *PloS one* **12** e0176674

[54] Allison B Z and Neuper C 2010 Could anyone use a bci? *Brain-computer interfaces* (Springer) pp 35–54

[55] Pfurtscheller G *et al.* 2010 *Frontiers in neuroscience* **4** 3

[56] Gabard-Durnam L J *et al.* 2018 *Frontiers in neuroscience* **12** 97

[57] Pan J and Tompkins W J 1985 *IEEE Trans. Biomed. Eng* **32** 230–236

[58] Citi L *et al.* 2012 *IEEE transactions on biomedical engineering* **59** 2828–2837

[59] Orini M *et al.* 2012 *IEEE Trans. on Biom. Eng.* **59** 663–673

[60] Pola S *et al.* 1996 *IEEE Transactions on Biomedical Engineering* **43** 46

[61] Al-Nashash H *et al.* 2004 *IEEE transactions on Biomedical Engineering* **51** 744–751

[62] Brennan M *et al.* 2002 *American Journal of Physiology-Heart and Circulatory Physiology* **283** H1873–H1886

[63] Catrambone V 2019 https://it.mathworks.com/matlabcentral/fileexchange/ 72704-brain-heart-interaction-indexes URL `https://it.mathworks.com/matlabcentral/fileexchange/72704-brain-heart-intera`

[64] Friston K J, Worsley K J, Frackowiak R S, Mazziotta J C and Evans A C 1994 *Human brain mapping* **1** 210–220

[65] Jekova I *et al.* 2008 *Medical Engineering and Physics* **30** 248–257

[66] Lu J *et al.* 2005 *nature* **435** 834

[67] Liu H and Yu L 2005 *IEEE Transactions on knowledge and data engineering* **17** 491–502

[68] Bengio Y and Grandvalet Y 2004 *Journal of machine learning research* **5** 1089–1105

[69] Shao J 1993 *Journal of the American statistical Association* **88** 486–494

[70] Rizzolatti G *et al.* 2004 *Annu. Rev. Neurosci.* **27** 169–192

[71] Tzagarakis C *et al.* 2010 *Journal of Neuroscience* **30** 11270–11277

[72] Pfurtscheller G *et al.* 2003 *Clinical neurophysiology* **114** 1226–1236

[73] Hagemann D *et al.* 2003 *Brain and cognition* **52** 79–87

[74] Thayer J F and Lane R D 2009 *Neuroscience & Biobehavioral Reviews* **33** 81–88

[75] Triggiani A *et al.* 2016 *International journal of psychophysiology* **103** 79–87

[76] Nagendra H *et al.* 2015 *Computational and mathematical methods in medicine* **2015**

[77] Porta A and Faes L 2013 *Philosophical transactions. Series A, Mathematical, physical, and engineering sciences* **371** 20120517–20120517

[78] Myrden A and Chau T 2015 *Frontiers in human neuroscience* **9** 308

[79] Molina G G *et al.* 2009 Emotional brain-computer interfaces *2009 3rd International Conference on Affective Computing and Intelligent Interaction and Workshops* (IEEE) pp 1–9

[80] Hoshi E and Tanji J 2007 *Current opinion in neurobiology* **17** 234–242

[81] Morasso P and Sanguineti V 1995 *Journal of Motor Behavior* **27** 52–66

[82] Catrambone V *et al.* 2018 Eeg processing to discriminate transitive-intransitive motor imagery tasks: Preliminary evidences using support vector machines *2018 40th Annual International Conference of the IEEE Engineering in Medicine and Biology Society (EMBC)* (IEEE) pp 231–234

[83] Catrambone V *et al.* 2018 Eeg complexity maps to characterise brain dynamics during upper limb motor imagery *2018 40th Annual International Conference of the IEEE Engineering in Medicine and Biology Society (EMBC)* (IEEE) pp 3060–3063